Stem Cell Reports
Article
ISSCR
OPEN ACCESS

Sodium Iodide Symporter PET and BLI Noninvasively Reveal Mesoangioblast Survival in Dystrophic Mice

Bryan Holvoet,[1] Mattia Quattrocelli,[2] Sarah Belderbos,[1] Lore Pollaris,[3] Esther Wolfs,[4] Olivier Gheysens,[1] Rik Gijsbers,[5] Jeroen Vanoirbeek,[3] Catherine M. Verfaillie,[6] Maurilio Sampaolesi,[2] and Christophe M. Deroose[1,*]

[1]Department of Imaging and Pathology, Nuclear Medicine and Molecular Imaging
[2]Department of Development and Regeneration, Translational Cardiomyology Lab
[3]Department of Public Health and Primary Care, Centre for Environment and Health
KU Leuven, Leuven 3000, Belgium
[4]Department of Morphology, Biomedical Research Institute, Lab of Histology, Universiteit Hasselt, Diepenbeek 3590, Belgium
[5]Department of Pharmaceutical and Pharmacological Sciences, Laboratory of Molecular Virology and Gene Therapy, Leuven Viral Vector Core
[6]Department of Development and Regeneration, Stem Cell Institute Leuven
KU Leuven, Leuven 3000, Belgium
*Correspondence: christophe.deroose@uzleuven.be
http://dx.doi.org/10.1016/j.stemcr.2015.10.018

SUMMARY

Muscular dystrophies are a heterogeneous group of myopathies, characterized by muscle weakness and degeneration, without curative treatment. Mesoangioblasts (MABs) have been proposed as a potential regenerative therapy. To improve our understanding of the in vivo behavior of MABs and the effect of different immunosuppressive therapies, like cyclosporine A or co-stimulation-adhesion blockade therapy, on cell survival noninvasive cell monitoring is required. Therefore, cells were transduced with a lentiviral vector encoding firefly luciferase (Fluc) and the human sodium iodide transporter (hNIS) to allow cell monitoring via bioluminescence imaging (BLI) and small-animal positron emission tomography (PET). Non-H2 matched mMABs were injected in the femoral artery of dystrophic mice and were clearly visible via small-animal PET and BLI. Based on noninvasive imaging data, we were able to show that co-stim was clearly superior to CsA in reducing cell rejection and this was mediated via a reduction in cytotoxic T cells and upregulation of regulatory T cells.

INTRODUCTION

Muscular dystrophies (MDs) are a heterogeneous group of muscle wasting diseases caused by impairment of the dystrophin-glycoprotein complex (DGC). This results in membrane fragility and contraction-mediated muscle injury. At present, no regenerative therapy for MDs is available and glucocorticoids are the only clinically accepted, disease-delaying drugs with serious long-term side effects (Bushby et al., 2010).

In healthy individuals, damaged muscles are restored by endogenous stem cells. This natural process of repair formed the basis of evaluating different stem cells for their regenerative potential in MDs. Our group has demonstrated that mesoangioblasts (MABs), which are vessel-derived stem cells, have therapeutic potential in several preclinical models of MDs (Sampaolesi et al., 2003, 2006). These positive results have led to a phase 1 clinical study in Duchenne (D)MD patients with HLA-matched MABs (EudraCT #2011-000176-33) (Cossu et al., 2015). Despite progress into clinical trial, limited information about the biodistribution and long-term survival of MABs in vivo is currently available.

To date, histology is the gold standard for evaluating stem cell engraftment in preclinical research. However, this is an invasive technique, which provides no whole body information, is prone to sampling errors, and hampers clinical translatability. Therefore, there is a need to noninvasively monitor stem cell location and survival. To allow long-term noninvasive cell monitoring, cells are indirectly labeled via incorporation of imaging reporter genes in the DNA of the cell and the encoded protein will specifically convert a substrate or bind and/or take up a reporter probe. This has some major advantages compared to direct labeling, as it allows long-term cell monitoring and reflects cell viability. Both factors are of crucial importance to evaluate and optimize stem cell therapy.

To visualize graft survival in vivo, mMABs were transduced with a lentiviral vector encoding a bicistronic imaging reporter gene construct encoding firefly luciferase (Fluc): Genbank: M15077 / PDB: 1LCI and human sodium iodide symporter (hNIS): Genbank: U66088 for optical and radionuclide imaging, respectively. The application of hNIS allows direct translation toward a clinical setting because it is of human origin and therefore immunologically neutral. Furthermore, it is a radionuclide reporter gene, as its protein product is capable of accumulating radioactive isotopes of iodine and pertechnetate ($^{99\ m}TcO_4^-$). This allows cell monitoring via clinically established noninvasive imaging approaches, namely positron emission tomography (PET) and single-photon emission computed tomography (SPECT) (Chung, 2002).

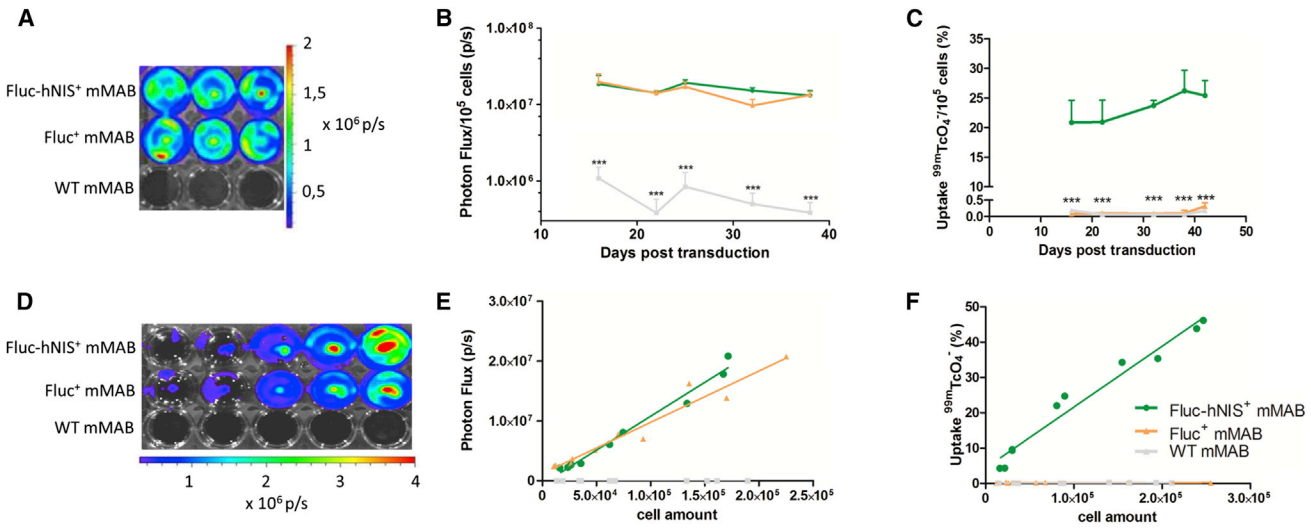

Figure 1. In Vitro Validation of Reporter Gene Expression in Undifferentiated Transduced mMABs

(A) Visualization of BLI signals in vitro.

(B) Quantitative analysis showed a high and stable BLI signal in both Fluc-hNIS$^+$ and Fluc$^+$ mMABs, which was significantly different compared to WT mMABs (***$p < 0.001$) (mean ± SD) (n = 5 IEs).

(C) Uptake experiments with $^{99m}TcO_4^-$ were also performed on different time points and only in Fluc-hNIS$^+$ mMABs a clear uptake (~23%) was observed which resulted in significant differences (****$p < 0.0001$) (mean ± SD) (n = 5 IEs).

(D) Visualization of BLI signals in vitro when seeded in different cell amounts clearly indicated an increase in BLI signals with increasing cell number in Fluc expressing mMABs.

(E) Quantitative analysis demonstrated a clear positive linear relationship between photon flux and cell amount in Fluc-hNIS$^+$ and Fluc$^+$ mMABs ($R^2 = 0.98$ and $R^2 = 0.94$).

(F) Also a positive linear correlation between $^{99m}TcO_4^-$ uptake and cell amount in Fluc-hNIS$^+$ mMABs was found ($R^2 = 0.96$), while no $^{99m}TcO_4^-$ uptake was present in Fluc$^+$ and WT mMABs.

To allow long-term cell survival of allogeneic MABs, donor rejection by the host should be avoided. To date, calcineurin inhibitors are standardly used in the clinic as immunosuppressive drugs despite their modest and variable results and numerous side effects (Fischer et al., 2011; Patel and Kobashigawa, 2004). Also, chronic immune suppressants render the patients prone to opportunistic infections. Therefore, the research field is evaluating short-term immune suppressants that induce donor tolerance. Several groups have demonstrated that by temporarily inhibiting the co-stimulatory signals, which are required for T cell activation, donor tolerance could be achieved (Huber et al., 2013; Murakami and Riella, 2014). In this project, a combination of two antibodies undergoing clinical evaluation (cytotoxic T-lymphocyte-associated protein 4-Ig, CTLA4-Ig and anti-lymphocyte function-associated antigen 1, anti-LFA1) will be used for co-stimulation adhesion blockade (co-stim) (Schiff et al., 2011; Vincenti et al., 2007).

Our goal for this study was to evaluate whether non-H2 matched mMABs injected in alpha-sarcoglycan null (*Sgca*$^{-/-}$) mice, which is a well-established model of MD, could be monitored via bioluminescence imaging (BLI) and small-animal PET (Duclos et al., 1998). Furthermore, we wanted to use these noninvasive imaging methods to assess the efficacy of different immune suppressants on long-term mMAB survival.

RESULTS

Fluc and hNIS Expression Was Functional and Had a Positive Linear Correlation with Cell Amount

GFP$^+$ mMABs were transduced with a lentiviral vector (LV) containing either a bicistronic imaging reporter gene construct expressing Fluc and hNIS or a unicistronic imaging reporter gene expressing Fluc alone. Only Fluc expressing mMABs were capable of showing a robust BLI signal (Fluc$^+$ mMABs 1.37 ± 0.43 × 10^7 total photon flux, p/s, and Fluc-hNIS$^+$ mMABs 1.48 ± 0.40 × 10^7 p/s), while only a background signal could be observed in wild-type (WT) mMABs (0.06 ± 0.03 × 10^6 p/s and $p < 0.001$) (Figure 1A). mMABs were maintained in culture and on all time points a BLI signal was produced in both transduced mMABs (Figure 1B). To evaluate the functionality of hNIS, cells were incubated with $^{99m}TcO_4^-$ and a clear tracer uptake of 23.42 ± 2.48% in Fluc-hNIS$^+$ mMABs was

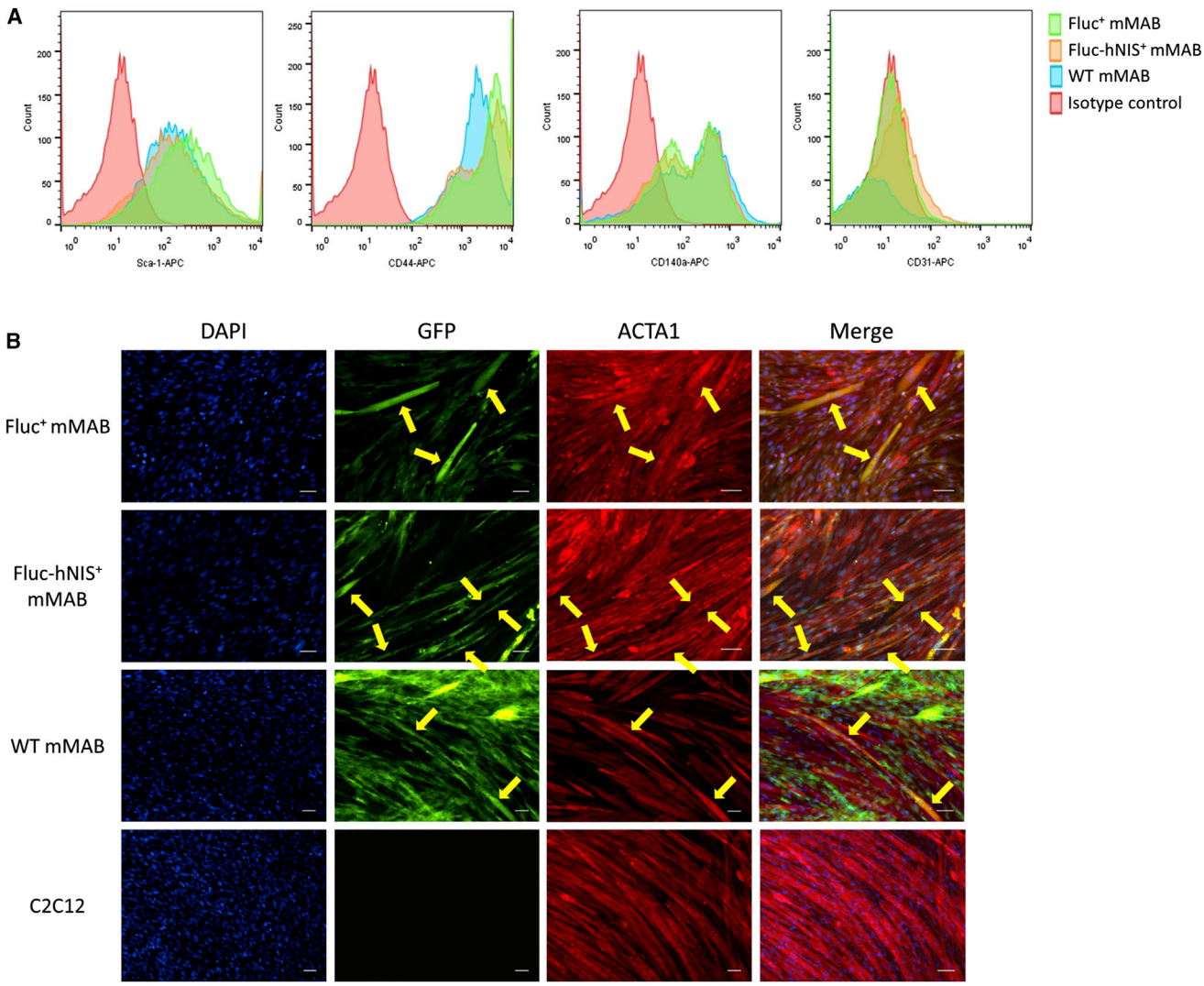

Figure 2. Maintained Cell Characteristics and Differentiation Capacity in Transduced mMABs

(A) No difference in expression of surface markers was observed between transduced mMABs and WT mMABs. All mMABs were positive for the typical markers (Sca-1, CD44, and CD140α) and negative for the endothelial marker CD31.

(B) Both transduced and WT mMABs were capable of fusing/differentiating toward myofibers, indicated via the presence of yellow fibers due to the overlay of GFP and red stained ACTA1. No GFP could be found in the myofiber differentiation of the C2C12s alone. The scale bar represents 100 μm.

observed, while no uptake was shown in Fluc$^+$ (0.14 ± 0.01%) and WT (0.11 ± 0.07%) mMABs on all time points ($p < 0.0001$) (Figure 1C).

To estimate cell survival in vivo, we investigated whether BLI signals and uptake percentages correlated with cell amounts. Therefore, mMABs were plated out in different cell amounts and both BLI signals as uptake percentages were determined. A clear positive linear correlation between cell amount and photon flux was shown both for Fluc$^+$ and Fluc-hNIS$^+$ mMABs ($R^2 = 0.94$ and $R^2 = 0.98$) (Figures 1D and 1E). Also the tracer uptake resulted in a positive linear correlation for Fluc-hNIS$^+$ mMABs ($R^2 = 0.96$) (Figure 1F). Again, no tracer uptake could be observed in Fluc$^+$ and WT mMABs.

Transduced mMABs Maintained Cell Characteristics and Myogenic Differentiation Capacity

The impact of the transduction process on the expression of mMAB cell surface markers was assessed via flow cytometry. Both transduced mMABs and WT mMABs were positive for typical mMAB surface markers including CD140α, CD44, and Sca-1 (Figure 2A). In contrast, both transduced and WT mMABs were negative for CD31, which is an endothelial marker (Figure 2A).

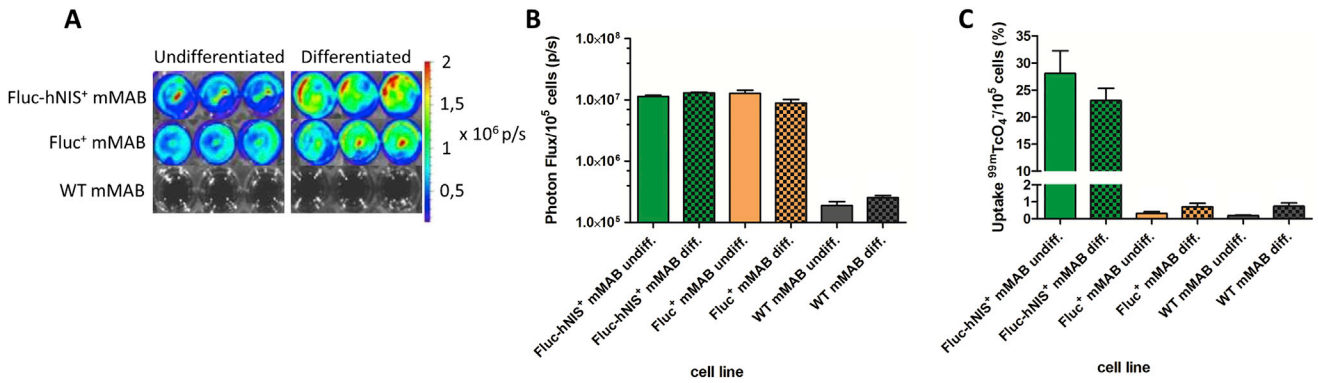

Figure 3. In Vitro Validation of Reporter Gene Expression in Differentiated Transduced mMABs

(A) Visualization of BLI signals in undifferentiated and differentiated mMABs indicated clear BLI signals in transduced mMABs in both conditions (n = 3 TR).

(B) Quantitative analysis of BLI signals indicated only a BLI signal in transduced mMABs. There was no difference that could be observed between BLI signals produced in undifferentiated and differentiated transduced mMABs after normalization to cell amount (mean ± SD).

(C) Quantitative analysis of tracer uptake demonstrated tracer uptake in both undifferentiated and differentiated Fluc-hNIS$^+$ mMABs (n = 3 TR). There was no difference that was observed between both conditions in the Fluc-hNIS$^+$ mMABs (mean ± SD).

Preservation of differentiation capacity of transduced mMABs toward myofibers was assessed via a co-culture experiment with C2C12s (Figure 2B). After 7 days of differentiation, cells were stained for GFP, skeletal muscle alpha 1 actin (ACTA1), which is a myogenic marker, and clear mMABs derived myofibers could be observed in all conditions.

Functional Reporter Gene Expression Was Maintained after Differentiation

When mMABs undergo differentiation, their gene expression profile changes and therefore the expression of our reporter genes needed to be re-evaluated (Figure 3). Clear BLI signals were again only observed in the transduced mMABs when D-Luciferin was administered in both differentiated (Fluc$^+$ mMABs 0.89 ± 0.12 × 10^7 p/s and Fluc-hNIS$^+$ mMABs 1.14 ± 0.60 × 10^7 p/s) and undifferentiated (Fluc$^+$ mMABs 1.28 ± 0.16 × 10^7 p/s and Fluc-hNIS$^+$ mMABs 1.30 ± 0.32 × 10^7 p/s) conditions. Furthermore, no difference in photon flux was observed between differentiated and undifferentiated mMABs after correction for cell amount (Figures 3A and 3B). Also the functionality of hNIS was assessed and even after differentiation 23.06 ± 2.27% of the tracer was taken up (fold increase compared to Fluc$^+$ and WT mMABs: 127) (Figure 3C).

Noninvasive Monitoring of Transduced mMABs via Small-Animal PET in *Sgca*$^{-/-}$ Mice

After in vitro validation of our transduced mMABs, 1 × 10^6 Fluc-hNIS$^+$ mMABs were bilaterally injected in the femoral arteries of *Sgca*$^{-/-}$ mice. To prevent rejection of the non-H2 matched mMABs, two different immune suppressant regimens were used, namely CsA and co-stim. Also a group receiving no immune suppression was included. CsA was administered chronically, while co-stim (consisting of CTLA4-Ig and anti-LFA1) was only administered on day 0, 2, 4, and 6, in accordance to the protocol of Huber et al. (2013).

First, we evaluated the functionality of hNIS in vivo via small-animal PET. On day 1 and 3 post-injection of the cells, iodide-124 ($^{124}I^-$) was injected intravenously. On both days, there was a clear tracer uptake in the hind limbs of cell-injected animals, while it was absent in sham-injected animals (Figures 4A–4C). Therefore, significantly higher standardized uptake values (SUVs) were observed in the hind limbs of cell-injected mice (co-stim day 1: 0.28 ± 0.14 and day 3: 0.13 ± 0.05; CsA day 1: 0.22 ± 0.07 and day 3: 0.14 ± 0.04; and no immuno day 1: 0.18 ± 0.02 and day 3: 0.14 ± 0.01) compared to sham-injected mice (co-stim day 1: 0.06 ± 0.01 and day 3: 0.05 ± 0.01; CsA day 1: 0.08 ± 0.02 and day 3: 0.05 ± 0.01; no immuno day 1: 0.06 ± 0.01 and day 3: 0.08 ± 0.01; $p < 0.05$; and $p < 0.01$) (Figure 4D). No differences in SUVs were present between the cell-injected animal groups.

Evaluating the Efficacy of Immune Suppressants via BLI

To evaluate the functionality of Fluc in vivo, BLI was performed on different days after injection (Figure 5). Clear BLI signals were present in all cell-injected mice, while only background signals were present in sham-injected animals (maximal photon flux: 3.1 ± 0.6 × 10^3 p/s/cm^2/steradian, sr). Until day 4, no significant differences in BLI signals could be observed between the different cell-injected groups (co-stim 27.40 ± 3.75 × 10^6 p/s/cm^2/sr; CsA

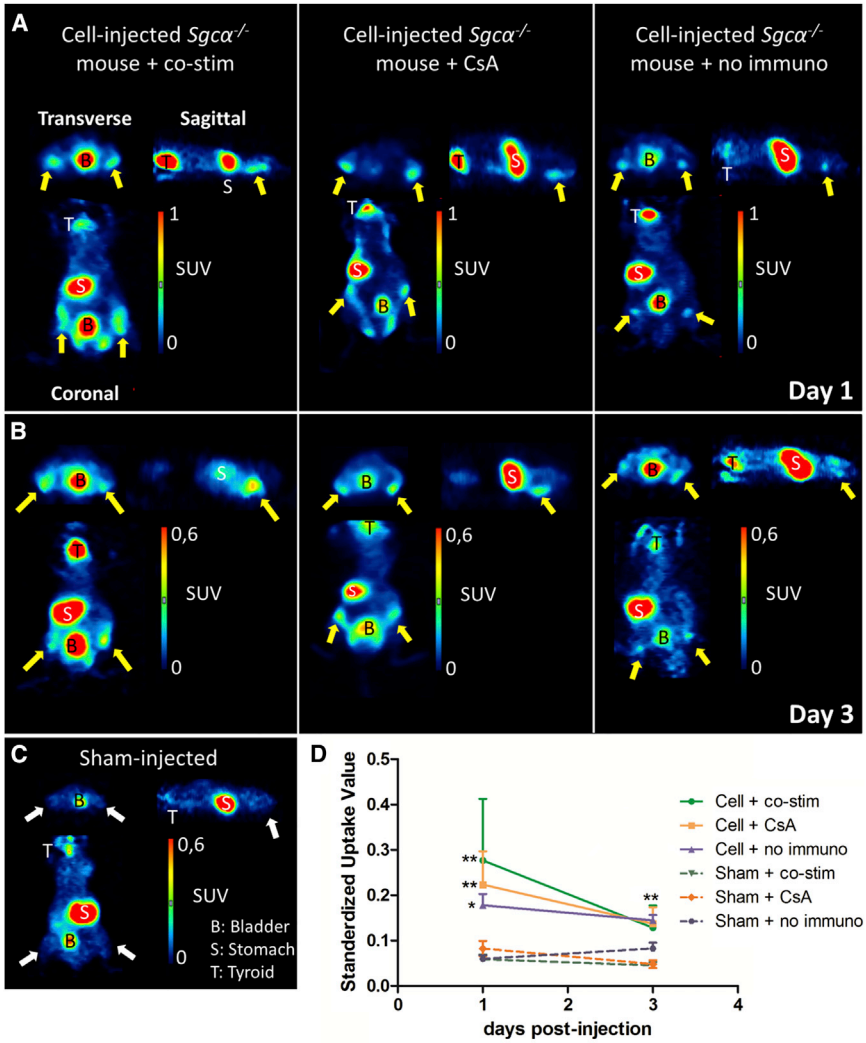

Figure 4. Visualization of Intraarterial Injected Fluc-hNIS$^+$ mMABs via Small-Animal PET

(A–C) 1 × 10^6 Fluc-hNIS$^+$ mMABs were injected bilaterally in the femoral arteries of *Sgca*$^{-/-}$ mice (n = 4 IR) without immune suppression or with co-stim or CsA as immune suppression. Sham-injected animals were also included for all groups (n = 3 IR). At 1 and 3 days after cell injection, $^{124}I^-$ was administered. Clear tracer uptake could be observed in the hind limbs of cell-injected animals (indicated via the yellow arrows) at day 1 (A) and day 3 post-injection (B), which was absent in sham-injected animals (indicated via the white arrows) (C). The regions where NIS was endogenously expressed (thyroid, T, and stomach, S) also were clearly visible, together with the bladder.

(D) Quantitative analysis clearly demonstrated significantly higher SUVs in the hind limbs of cell-injected animals compared to sham-injected animals (**p < 0.01 and *p < 0.05) without significant differences between the different cell-injected groups (mean ± SD).

14.14 ± 2.63 × 10^6 p/s/cm^2/sr; and no immuno 3.24 ± 0.9 × 10^6 p/s/cm^2/sr). At day 7, a significantly higher cell survival was observed in cell-injected animals with immune suppression (co-stim 14.17 ± 2.44 p/s/cm^2/sr and CsA 10.31 ± 3.20 p/s/cm^2/sr) compared to cell-injected animals without immune suppression (0.40 ± 0.12 × 10^6 p/s/cm^2/sr and $p < 0.05$). In the animal groups receiving CsA as immune suppression, a significantly lower cell survival was observed compared to animals receiving co-stim at day 10 post-injection (CsA 2.5 ± 0.7 × 10^4 p/s/cm^2/sr and co-stim 2.93 ± 0.62 × 10^6 p/s/cm^2/sr). This significant increase in cell survival in *Sgca*$^{-/-}$ under co-stim immune suppression remained until day 14 post-injection ($p < 0.05$). However, stable cell survival was not achieved in *Sgca*$^{-/-}$ mice under either immunosuppressive regimen. The latest time point where mMABs could still be detected in *Sgca*$^{-/-}$ mice with co-stim was day 21 post-injection.

Monitoring mMAB Survival in Nude Mice via Small-Animal PET and BLI

To assess the impact of the immune system we studied nude mice, which have a deficiency in T cell function. Cardiotoxin was administered to the hind limb muscles to generate an acute model of muscle damage and regeneration. In these mice (n = 10), we injected the right hind limb with Fluc-hNIS$^+$ mMABs, while in the left hind limb Fluc$^+$ mMABs were injected as a negative control for our small-animal PET.

After intravenous tracer injection, a clear signal could be observed in the right hind limb on day 1 and day 3 post-injection (day 1: 0.17 ± 0.04 and day 3: 0.11 ± 0.01), while it was absent in the left hind limb (day 1: 0.07 ± 0.03 and day 3: 0.07 ± 0.02) (Figures 6A and 6B). This resulted in significantly higher SUVs in the right hind limbs compared to the left hind limbs ($p < 0.001$) (Figure 6B).

We also performed cell monitoring via BLI in these mice and since both mMABs express Fluc, both cell grafts were

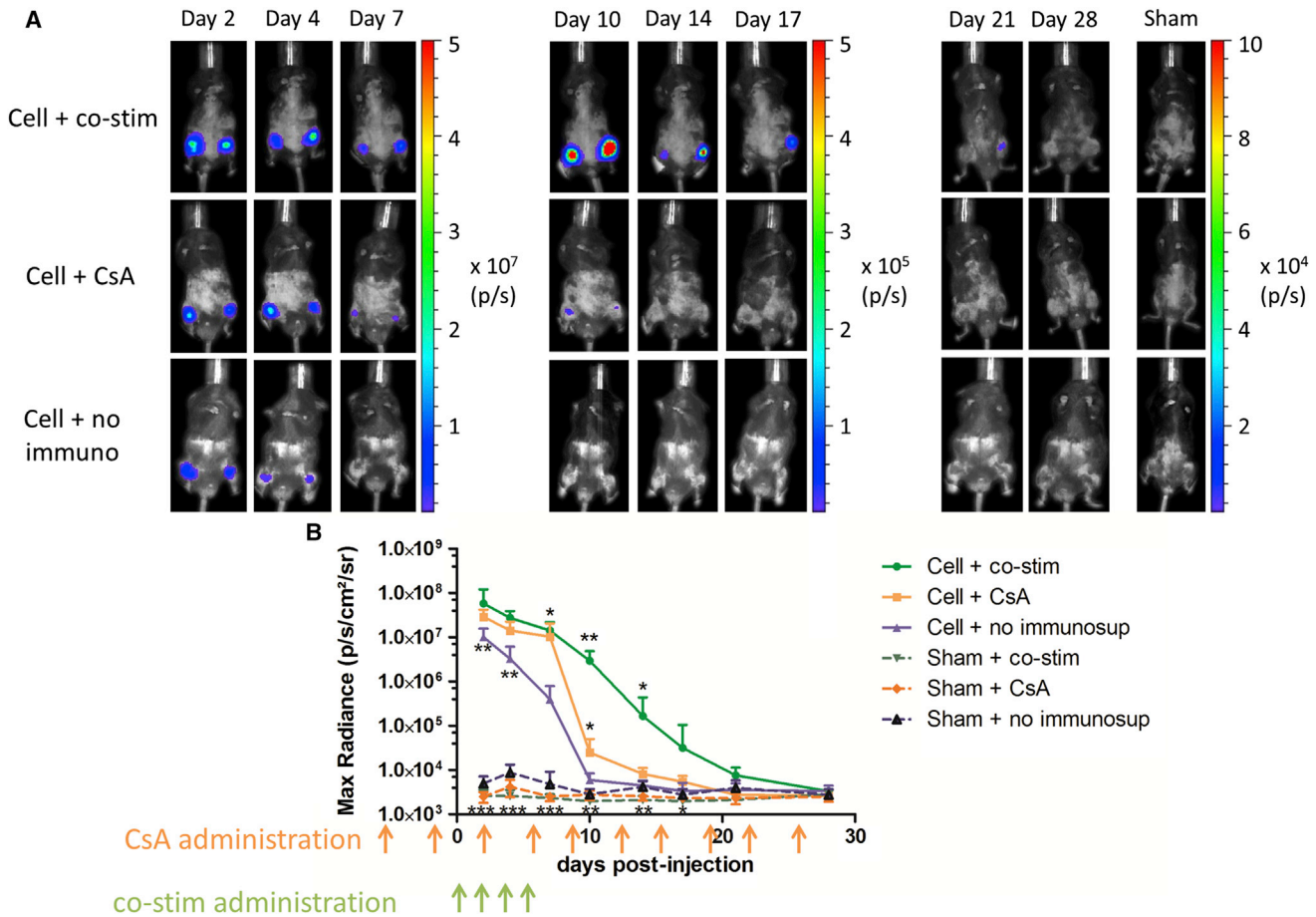

Figure 5. Monitoring of Intraarterial Injected Fluc-hNIS$^+$ mMABs via BLI

(A) 1 × 10^6 Fluc-hNIS$^+$ mMABs were injected bilaterally in the femoral arteries of *Sgca*$^{-/-}$ mice without immune suppression (n = 5 IR) or with co-stim or CsA as immune suppression (n = 6 IR). Sham-injected animals were also included for all groups (n = 5 IR). Robust BLI signals were present in all cell-injected animals the first days after injection, while only background signal was observed in sham-injected animals. (B) Quantitative analysis demonstrated that starting from day 7, significantly higher BLI signals were present in cell-injected animals receiving immune suppression compared to cell-injected animals not receiving immune suppression (*$p < 0.05$). Starting from day 10 until day 14, significantly higher cell survival was shown in animals receiving co-stim compared to CsA as immune suppressant (**$p < 0.01$ and *$p < 0.05$) (mean ± SD). Cells were lost in animals without immune suppression at 10 days post-injection, at day 14 post-injection in animals with CsA, and at day 28 for animals receiving co-stim (see also Figure S2).

clearly visible (Figure 6C). In these nude mice, we were able to longitudinally monitor the mMABs for 4 months via BLI. After an initial cell decrease, stable cell survival was achieved as indicated by the presence of a stable BLI signal after 21 days. Also, no difference in cell survival could be observed between hNIS$^+$ and hNIS$^-$ mMABs (Figure 6D). Ex vivo BLI and histological assessment in another cohort demonstrated the engraftment of the mMABs in the gastrocnemius muscles (Figure S1).

Evaluation of the Immunological Status of the *Sgca*$^{-/-}$ Mice

The fact that only in nude mice mMABs survived for longer than 4 months and not in the *Sgca*$^{-/-}$ mice indicates involvement of the adaptive immune system in cell death or survival. To assess the immunological status of the *Sgca*$^{-/-}$ mice under different immune suppressive regimens, the T cells were isolated from the spleen and the fraction of T helper cells (CD3$^+$CD4$^+$ cells), cytotoxic T cells (CD3$^+$CD8$^+$ cells), and activated/regulatory T cells (Tregs; CD3$^+$CD4$^+$CD25$^+$ cells) were evaluated (Figure 7). The fraction of T helper cells was similar in all groups (cell-injected no immuno 49.13 ± 11.27%; CsA 46.81 ± 3.53%; co-stim 51.99 ± 5.36%; sham-injected no immuno 46.53 ± 10.05%; CsA 56.25 ± 6.46%; and co-stim 55.38 ± 2.68%) (Figure 7A). The cytotoxic T cells were significantly increased in all cell-injected animals (no immuno 31.73 ± 2.85%; CsA 32.23 ± 4.98%; and co-stim 22.95 ± 4.28%)

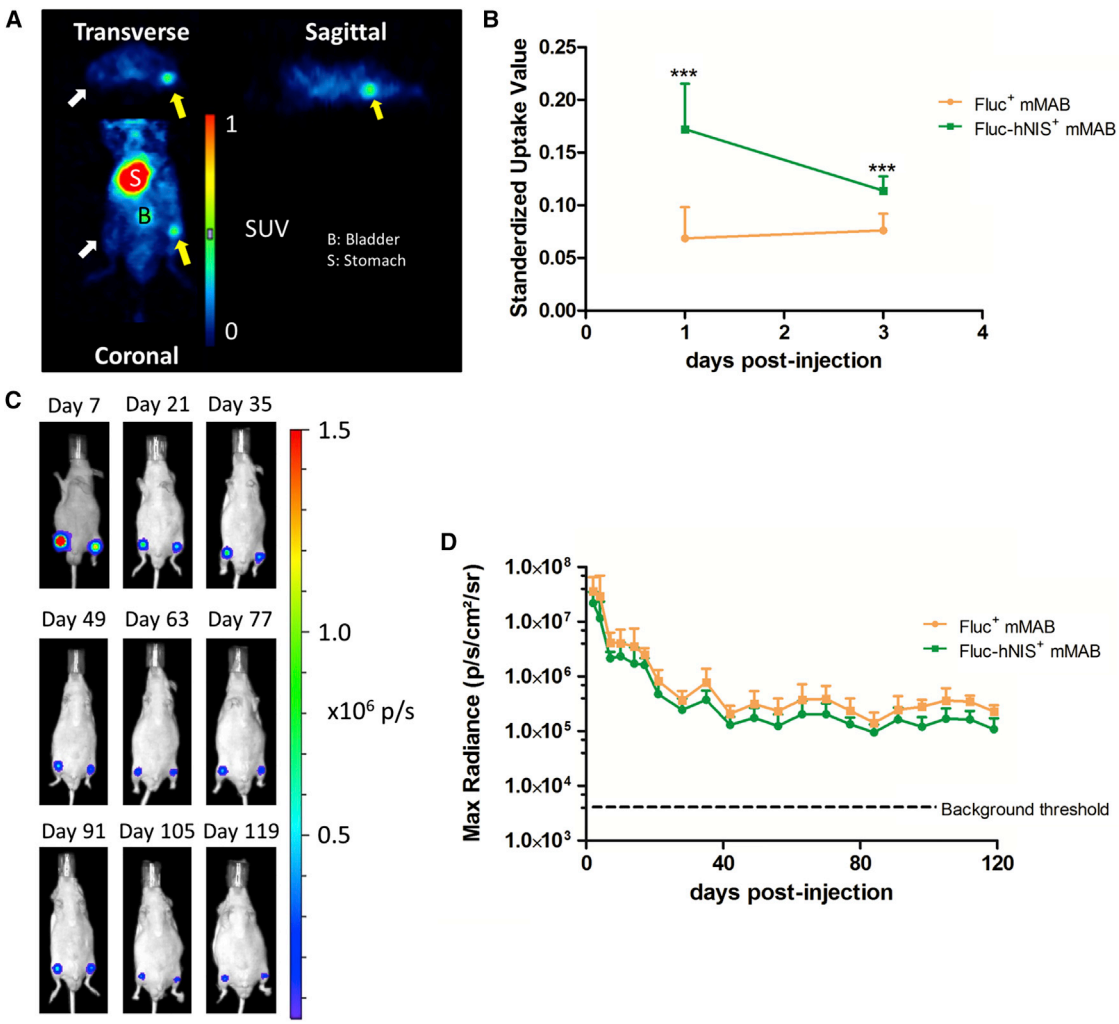

Figure 6. Monitoring of Intraarterial Injected Fluc$^+$ and Fluc-hNIS$^+$ mMABs via BLI and Small Animal PET

(A) 1 × 10^6 Fluc$^+$ and Fluc-hNIS$^+$ mMABs were injected in the left and right femoral artery, respectively, of nude mice with acute muscle damage (n = 10 IR). After $^{124}I^-$ administration only in the right hind limbs, the Fluc-hNIS$^+$ cells could be detected, while background signal was present in the left hind limbs (representative image of day 1 post-injection).

(B) Quantitative analysis resulted in significantly increased SUVs in the right hind limbs compared to the left hind limbs both on day 1 and day 3 (***$p < 0.001$) (mean ± SD).

(C) Representative BLI images indicate the feasibility to monitor both Fluc$^+$ and Fluc-hNIS$^+$ mMABs longitudinally via BLI.

(D) Quantitative analysis demonstrated a robust BLI signal, which remained stable starting from day 21 (mean ± SD) (see also Figure S1).

compared to sham-injected animals (no immuno 23.9 ± 3.61%; CsA 24.5 ± 5.3%; co-stim 15.72 ± 1.26%; and $p < 0.05$) (Figure 7B). *Sgca*$^{-/-}$ mice with co-stim had a significantly lower fraction of cytotoxic T cells compared to *Sgca*$^{-/-}$ mice treated with CsA or without immune suppression ($p < 0.05$ and $p < 0.01$). For the Tregs, there was a significant increase in the animals under co-stim (cell 2.35 ± 0.78% and sham 2.15 ± 0.75%) compared to injected *Sgca*$^{-/-}$ mice given CsA (cell 0.75 ± 0.29% and sham 1.1 ± 0.21%) or without immune suppression (cell 0.60 ± 0.26% and sham 0.60 ± 0.27%) (Figure 7C).

mMAB Survival Correlates with Improved Running Distance of *Sgca*$^{-/-}$ Mice

To evaluate the potential beneficial effects of the cell-injected animals, *Sgca*$^{-/-}$ mice ($n \geq 5$) were placed on a treadmill with increasing speed (1 m/min every minute). The results are shown as relative improvement (%), namely, increased running distance (Δm) normalized to baseline (Figures S2A and S2B). At day 14 post-injection, only cell-injected *Sgca*$^{-/-}$ mice receiving co-stim had an increased running distance of 104 ± 43% normalized to baseline. No improvement in running distance was

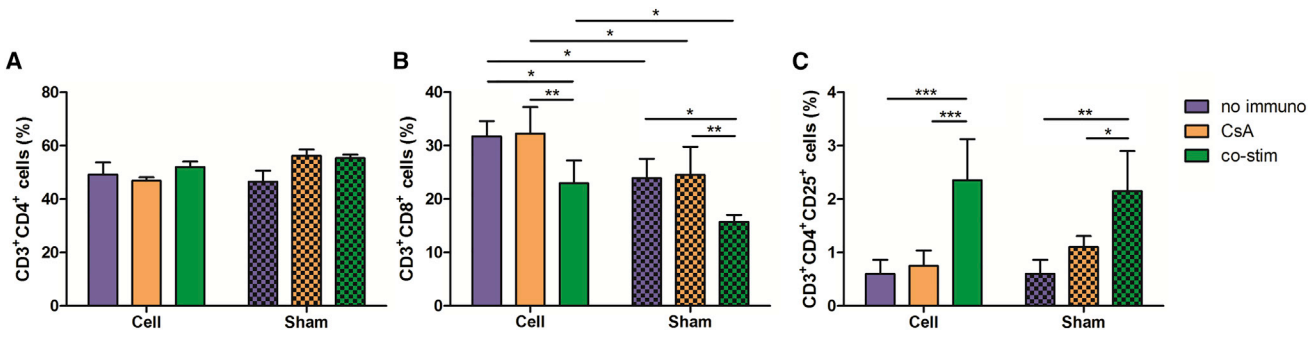

Figure 7. Evaluation of T Cell Populations in *Sgca*$^{-/-}$ Mice

(A) No significant differences in T helper cells could be observed between the different groups ($n \geq 5$ IR) (mean ± SD).

(B) A significant increase in cytotoxic T cells was present in cell-injected animals compared to sham-injected animals for all groups (*$p < 0.05$) ($n \geq 5$ IR). Also, a significant decrease in cytotoxic T cells was observed in animals with co-stim as immune suppressant compared to the other groups (*$p < 0.05$ and **$p < 0.01$) (mean ± SD). There was no difference that was observed between animals without immune suppression and with CsA as immune suppression.

(C) Co-stim as immune suppressant generated a significantly higher population of Tregs compared to the other groups (*$p < 0.05$; **$p < 0.01$; and ***$p < 0.001$) (mean ± SD) ($n \geq 5$ IR). Again, there was no difference that was observed between animals without immune suppression and with CsA as immune suppressant.

observed in the other cell-injected animals (CsA −34 ± 16% and no immuno 6 ± 20%) or sham-injected animals (co-stim 17 ± 35%; CsA −24 ± 14%; no immuno −42 ± 14%; and $p < 0.01$). At day 28 post-injection, none of the groups showed signs of improvement. On ex vivo BLI, Fluc-hNIS$^+$ mMABs could be retrieved in the gastrocnemius of cell-injected animals receiving co-stim at day 14 post-injection, while no mMABs were found in the other groups (Figure S2C). At day 28, none of the groups could visualize the cells on ex vivo BLI (Figure S2D). Histological assessment showed the presence of GFP$^+$ fibers expressing SGCA in the co-stim suppressed group, while the other groups had no GFP$^+$ fibers at day 14 post-injection (Figure S2E). Also on histological assessment at day 28 post-injection, the cells could not be retrieved in all groups (Figure S2F).

DISCUSSION

MABs are vessel-derived stem cells with a high regenerative potential for MDs. Sampaolesi et al. (2003, 2006) have demonstrated that MABs are capable of partially restoring the DGC in preclinical models of MD and reducing the associated loss in muscle strength in these animals. The positive results obtained in these studies have led to a phase 1 clinical trial (EudraCT #2011-000176-33) in DMD patients (Cossu et al. 2015). Despite this initial translation into the clinic, limited information on MAB survival and distribution is currently available in vivo. Also, the effect of different immune suppressants on MAB survival after systemic administration has not been investigated. Therefore, the research field would benefit from novel techniques to longitudinally and noninvasively monitor cell survival. We used an indirect labeling approach, which allows the monitoring of mMABs via BLI and PET in *Sgca*$^{-/-}$ mice and an acute muscle damage and regeneration immune-deficient mouse model.

The indirect labeling approach for cell tracking was used as it has three major advantages compared to the most commonly used direct labeling approach. First, only viable cells are capable of expressing the reporter genes. Second, the detected imaging signals clearly correlate with cell amount, as demonstrated in our in vitro experiment. Third, repeated administration of the tracer can be performed to allow long-term monitoring. These three properties are of crucial importance to evaluate cell-mediated therapy. Long-term monitoring of cell viability is required for regenerative purposes and monitoring of cell growth is important as a safety measurement for pluripotent-derived cells, which have the risk of forming teratomas.

For mMAB visualization, we have opted to integrate both an optical (Fluc) and a human radionuclide (hNIS) imaging reporter gene in the genomic DNA of the host cells via LVs (Sakuma et al., 2012). BLI has a very high sensitivity and is virtually background-free. Therefore, it is capable of detecting very low cell amounts in vivo. However, it is limited to preclinical research since the signal produced is visible light. PET has as major advantage the direct translation toward a clinical setting. The disadvantage is the lower sensitivity compared to BLI, however, the sensitivity is still higher than other clinical devices (Massoud and Gambhir, 2003). The most commonly used radionuclide reporter gene is the herpes simplex virus type 1 thymidine kinase,

which has a viral origin and therefore may induce immunological reactions (Gambhir et al., 1999). In this study, we have used hNIS, which has no potential immunological consequences due to its human origin (Chung, 2002). Due to the restricted endogenous expression of NIS (thyroid, stomach, salivary, and mammary glands), hNIS-based cell monitoring is feasible in the majority of the body. These advantages have resulted in several preclinical cell monitoring studies (Lee et al., 2013, 2015a, 2015b; Templin et al., 2012; Wolfs et al., 2014).

We demonstrated that hNIS and Fluc were functional and remained stably expressed in vitro, even after differentiation. Furthermore, a clear correlation between imaging signals and cell number was observed in vitro, which is a prerequisite to noninvasively evaluate cell survival in vivo. Finally, genomic integration of the reporter gene construct did not induce any alterations to the cell's characteristics or differentiation capacity. Therefore, we can conclude that we have generated a stable stem cell line expressing imaging reporter genes without altering the functionality of the cells.

Afterward, Fluc-hNIS^{+} mMABs were bilaterally injected into the femoral arteries and successfully monitored via both BLI and small-animal PET. After systemic administration, we were clearly able to monitor mMABs for several days via small-animal PET. Long-term cell monitoring was not feasible because of cell loss over time and the lower sensitivity of PET compared to BLI (Massoud and Gambhir, 2003). To overcome this limitation, more potent promoters combined with enhancers need to be used to increase the expression levels of the reporter gene (Minn et al., 2014).

One other imaging study has been performed for MAB therapy of MDs. In this study, a direct cell labeling approach via iron nanoparticles was performed to monitor the cells via MRI (Odintsov et al., 2011). This cell labeling approach is limited by contrast agent dilution, no discrimination between viable and nonviable cells, and nonspecific uptake by macrophages (Li et al., 2008). In the study of Odintsov et al. (2011) iron oxide labeled MABs were injected in mdx mice and nonspecific uptake of nanoparticles by the macrophages was observed. Furthermore, they were not able to visualize mMABs after systemic delivery.

At present, a major limitation for cell transplantation is cell rejection by the host (Alpdogan, 2013). Contrasting results have been found for MABs and their reaction with the immune system. English et al. (2013) demonstrated that human MABs are capable of suppressing T cell proliferation. Guttinger et al. (2006) also observed no activation of T cells after stimulation with mMABs. However, isolated T cells from mMAB-injected muscles were clearly reactive against re-exposure to mMABs. Noviello et al. (2014) also indicated that human MABs exposed to inflammatory conditions or during differentiation are capable of inducing T cell expansion and are becoming sensitive to T cell mediated killing.

In this study, we were able to noninvasively monitor non-H2 matched mMAB survival and to evaluate both the reaction of mMABs with the immune system and the efficacy of different immune suppressants. This imaging-based assessment has already been demonstrated to be successful by several other groups (Everaert et al., 2012; Gheysens et al., 2006; Huber et al., 2013). Currently, chronic immunosuppressive therapy is the gold standard, but has modest and variable results in patients and lifelong immunosuppression makes them prone for secondary malignancies and opportunistic infections (Fischer et al., 2011). CsA is a widely used clinical immune suppressant that blocks T cell activation via blocking of cytokine gene expression, including interleukin (IL)-2 and IL-4 (Krönke et al., 1984). However, it is associated with numerous side effects and variable results in suppressing graft rejection have been observed (Fischer et al., 2011; Gheysens et al., 2006; Huber et al., 2013; Patel and Kobashigawa, 2004). Therefore, novel methods with only short-term suppression of the immune system are currently under investigation (Alpdogan, 2013).

Huber et al. (2013) demonstrated that a short regimen of co-stim (consisting of CTLA4-Ig and anti-LFA-1) outcompetes CsA in maintaining cell survival after intramuscular and intracardiac injection of human embryonic stem cell (hESC)-derived endothelial cells or hESC-derived cardiomyocytes, respectively. Co-stim functions via the inhibition of the co-stimulatory signals that are required for proper T cell activation. CTLA4-Ig has a higher affinity for CD80 and CD86, which are present on antigen presenting cells (APCs), and therefore blocks the CD28-CD80 or CD86 pathway, which is important for T cell stimulation (Boise et al., 1995). Anti-LFA-1 is responsible for the blocking of the LFA-1-ICAM-1 pathway and inhibits T cell activation (Nicolls et al., 2000). It has been demonstrated that the ICAM-1 pathway played a major role in the sensitivity of MABs toward T cell mediated rejection (Noviello et al., 2014).

Our BLI data demonstrated a slower decrease in cell viability in co-stim treated animals compared to *Sgca*$^{-/-}$ mice without immune suppression or treated with CsA. This improved cell survival under co-stim, and the inability of CsA to improve cell survival has also been demonstrated by others (Everaert et al., 2012; Gheysens et al., 2006; Huber et al., 2013). The relative stable cell survival the first days after injection followed by a drastic reduction is indicative of the role of the adaptive immune system. This is in line with previous publications indicating the importance of T cells in graft rejection (Rosenberg et al., 1987; Strom et al., 1975). Despite the beneficial effects of co-stim, stable

cell survival could not be achieved for more than 21 days post-injection, which is 15 days after stopping co-stim immune suppression.

A similar co-stim approach using adenoviral mediated muscle gene transfer by Adriouch et al. (2011) also failed to demonstrate long-term gene expression. Huber et al. (2013), however, were able to demonstrate stable cell survival only after local administrations, either intramuscular or intracardiac injections, in healthy animals. In contrast, cell survival in an acute myocardial infarction model was drastically reduced, highlighting the importance of the micro-environment for cell survival. In our study, a chronic dystrophic model with concomitant chronic inflammation was used, which reflects a hostile environment for transplanted cells. The latter may partly explain the limited cell survival.

We further studied the effect of the different immune suppressants on the immune system and analyzed the T cell populations of the spleen of the *Sgca*$^{-/-}$ mice. In all cell-injected animals a clear increase in cytotoxic T cells could be observed compared to sham-injected animals, in accordance with previous studies (Rosenberg et al., 1987; Strom et al., 1975). Also, a lower percentage of cytotoxic T cells was observed in animals suppressed with co-stim compared to the other groups. Kitchens et al. (2012) also observed a reduction in graft specific CD8^{+} T cells after immune suppression with only anti-LFA-1. Furthermore, an increase in Tregs in mice suppressed with co-stim was demonstrated. Tregs are well known for their ability to prevent autoimmunity and have been implicated in reducing allograft rejection after transplantation (Anderton and Liblau, 2008; George et al., 2008; Sakaguchi et al., 1995) Therefore, we can conclude that the immune system clearly interacts and rejects the non-H2 matched mMABs, with the cytotoxic T cells as major players for the immunological clearance. Also, co-stim is a better immune suppressant than CsA, since it is capable of reducing the number of cytotoxic T cells and increasing the number of Tregs.

The impact of T cell mediated cell killing could also be demonstrated via the evaluation of the running distance in mMAB treated animals. At day 14 post-injection, improvement of running distance was only present in mMAB-injected animals with co-stim, which were also the mice with the strongest mMAB survival at that time point. This indicates the importance of a sufficient number of surviving transplanted cells to obtain functional improvement. The other cell-injected groups had a drastically lower cell amount (20-fold) and hence had no functional improvement. Since cell survival was not maintained for more than 21 days, the improvement observed at day 14 was lost 28 days post-injection.

The cell injections were repeated in immune-deficient mice, which were given cardiotoxin intramuscularly to generate an acute model of muscle damage and regeneration. Stable and long-term cell survival could be observed via BLI. This furthermore indicated the potential of mMABs as a regenerative cell type for MDs. It also demonstrates the crucial role of the immune system in cell survival.

The limitations of our study are the inability to detect very low cell amounts via the imaging techniques (<500 cells for BLI; $< 1 \times 10^5$ cells for small-animal PET) and the potential increased immunogenicity of the cells because of reporter gene expression. However, the sensitivity of BLI might be sufficient to detect biologically significant cell survival, and the additive values of noninvasive cell monitoring still outweigh the invasive golden standard. And once in a clinical setting, only hNIS will be used and since this is a human radionuclide reporter gene, no immune response against the reporter gene product will occur.

Conclusion

In this study, we noninvasively monitored mMABs via BLI and small-animal PET in animal models of MD. The presence of a human radionuclide reporter gene allows cell detection in a clinical setting and therefore can help optimize stem cell therapies for MD. Our imaging approach allows assessing the efficacy of different immune suppressants on cell rejection. In this study, we showed that co-stim was significantly superior to CsA, even though the effect is only transient. Furthermore, we demonstrated that mMABs are susceptible to cytotoxic T cell mediated cell death in an inflammatory environment and that co-stim exerts its beneficial effects on cell death by reducing cytotoxic T cells and increasing Tregs.

EXPERIMENTAL PROCEDURES

Cell Culture

C2C12s (Sigma-Aldrich) and mMABs were cultured at 37°C in a 5% CO_2 humidified incubator under normoxic conditions. C2C12 growth medium (GM) consisted of DMEM, 10% heat-inactivated fetal bovine serum (FBS), 1% L-glutamine, 1% Penicillin Streptomycin (Pen-Strep) and 1% sodium pyruvate. And mMAB GM consisted of DMEM supplemented with 20% FBS, 1% Pen-Strep, 1% L-glutamine, 1% sodium pyruvate, 1% nonessential amino acids, and 0.2% β-mercaptoethanol. All GM components were obtained from Life Technologies.

First, transposon integration of CAGGS-GFP in the mMABs was achieved with a Sleeping Beauty Transposon (Quattrocelli et al., 2014).

There were two multicistronic LVs that were obtained from the Leuven Viral Vector Core (KU Leuven). In the first vector, the human elongation factor 1 alpha (hEF1a) drives the expression of the triple FLAG tagged Fluc (3FLAGFluc), *Thosea asigna* virus 2A (T2A), hNIS, and a puromycin resistance gene (PuroR) (LV_hEF1a-3FLAGFluc-T2A-hNIS-IRES-PuroR). The second vector

only contains Fluc and PuroR (LV_hEF1a-3FLAGFluc-IRES-PuroR). The mMABs were transduced with these LVs by incubating the cells with the vector (P24: 4.68 × 10^5 pg/10^5 cells for LV_hEF1a-3 FLAG Fluc-T2A-hNIS-IRES-PuroR and P24: 3.1 × 10^5 pg/10^5 cells LV_hEF1a-3FLAGFluc-IRES-PuroR) for 2 days and afterward selected by supplementing the GM with 1.5 μg/ml puromycin (Merck Millipore).

In Vitro Experiments

In Vitro Tracer Uptake

WT, Fluc$^+$ or Fluc-hNIS$^+$ mMABs were plated in triplicate under growth and differentiation medium. At the day of analysis, cells were incubated with $^{99\ m}TcO_4^-$ tracer solution (0.74 MBq/ml in DMEM) for 1 hr. Afterward, cells were rinsed with ice-cold PBS and supernatant was collected. The cells were lysed and collected. The radioactivity of the pellet and supernatant was measured by 2480 Wizard^2 Automatic Gamma Counter (PerkinElmer). The results were adjusted for tracer decay. Uptake values were corrected for cell amounts in the according samples as measured via the NucleoCounter NC-100 system (ChemoMetec).

In Vitro BLI

WT, Fluc$^+$, or Fluc-hNIS$^+$ mMABs were plated in triplicate under growth and differentiation medium. At day of analysis, 0.3 mg/l D-Luciferin (Promega, Benelux) was added to the mMABs and the emitted light photons were detected with the IVIS Spectrum (Caliper Life Sciences). The signal was corrected for cell number and expressed as p/s per 10^5 cells. In vitro BLI signals were analyzed with Living Image version 4.2 (Caliper Life Sciences).

Immunohistochemistry

Samples were fixed with 4% paraformaldehyde (PFA) (Kodak) in PBS for 15 min, rinsed, and subsequently incubated with 0.2% triton (Triton X-100, Sigma-Aldrich) in 1% BSA in 1× PBS (Sigma-Aldrich) for 30 min. Samples were again rinsed and afterward donkey serum (1/10 diluted in 1% BSA, VWR) was added for 60 min. Next, samples were incubated with primary antibodies diluted in 1% BSA, goat anti-GFP (1/500, # ab6673, Abcam) and rabbit anti-ACTA1 (1/300, #ab50591, Abcam) overnight at 4°C. The following day, samples were rinsed and incubated with the secondary antibodies anti-goat 488 and anti-rabbit 594 Alexa Fluorphore (both 1/500 in 1% BSA, #Z25002, #Z25307, Life Technologies) for 1 hr at room temperature (RT). Samples were rinsed and counterstained using DAPI (10 μg/ml in 1% BSA, Sigma-Aldrich). Afterward, samples were analyzed with an Eclipse TI fluorescence inverted microscope (Nikon) using NIS Elements AR 4.11.01 software (Nikon).

Animals

All experiments were approved by the Ethical Committee of the KU Leuven. Age-matched *Sgca*$^{-/-}$ mice (C57/Bl6 background, 4 months old) were generated by our group. There were 6-week-old thymic aplasia nude (NMRI-nu) mice that were obtained from Janvier Labs and received a 10 μM solution of cardiotoxin (*Naja Mossambica Mossambica*, Sigma-Aldrich) in the tibialis anterior, gastrocnemicus, and quadriceps muscle of each hind limb.

During manipulations and imaging procedures, mice were anaesthetized using 2% or 3% isoflurane (IsoVET, 100 mg/g, Eurovet, Piramal Healthcare) in 100% O_2 (2 l/min) for *Sgca*$^{-/-}$ or nude mice, respectively. There were one million mMABs that were injected in physiological water supplemented with 1/10^4 heparin (Heparine LEO, 5.000 I.E./ml, LEO Pharma A/S) bilaterally into the femoral arteries. Control animals underwent a sham operation.

Sgca$^{-/-}$ mice either received no immunosuppressive therapy, intraperitoneal (i.p.) CsA (10 μl/g, Neoral Sandimmum, Novartis) twice weekly starting 1 week before transplantation, or i.p. co-stim (consisting of anti-LFA-1 and CTLA-4-Ig) according to the protocol described by Huber et al. (2013). Anti-LFA-1 antibody and CTLA-4-Ig were bought from BioXCell.

In Vivo Imaging

Small-Animal PET

The mice received an intravenous injection of 3.7–5.55 MBq ^{124}I (PerkinElmer) on day 1 and 3 and an intramuscular injection of 100 μl LASIX (20 mg/ml, Sanofi) as diuretic. At 3 hours later, a 20 min static scan was acquired with the Focus 220 small-animal PET system (Siemens Medical Solutions USA). A transmission scan was acquired using a ^{57}Co source (5 mCi, Eckert and Ziegler). PET images were reconstructed using a maximum a posteriori (MAP) image reconstruction algorithm and were then analyzed with PMOD 3.0 (PMOD technologies). SUV was calculated according to the following formula:

$$SUV = \frac{Activity\ concentration\ in\ organ}{\left[Injected\ activity / weight\ of\ animal\right]}.$$

Volumes of interest were manually positioned around the graft regions.

BLI

For in vivo BLI scans, mice were placed in the flow chamber of IVIS Spectrum. Subsequently, 126 mg/kg of D-Luciferin was injected subcutaneously. Next, consecutive frames were acquired until the maximum signal intensity was reached. Region of interests were drawn around the regions injected with Fluc$^+$ or Fluc-hNIS$^+$ mMABs and the maximal radiance (p/s/cm^2/sr) was measured within these regions. Images were analyzed using Living Image version 4.2.

T Cell Isolation

The spleens of *Sgca*$^{-/-}$ mice were isolated and a single cell suspension in ice-cold RPMI 1640 medium (Life Technologies) was generated via a 100 μm falcon cell strainer (Corning Life Science DL). The samples were then centrifuged at 300 *g* for 10 min at 4°C. Next the pellet was resuspended in ammonium-chloride-potassium (ACK) lysing buffer (Life Technologies) for 5 min at RT and centrifuged at 300 *g* for 5 min at 21°C. The cells were resuspended in ice-cold MACS buffer (0.5% BSA and 2 mM ethylenediaminetetraacetic acid, Sigma-Aldrich, in PBS) and magnetic labeling and separation of the CD3$^+$ T cells were performed according to the following protocol: "CD3ε MicroBead Kit, mouse" (MACS Miltnyi Biotec). T cells were fixed with 2% PFA for 15 min, centrifuged at 1,000 *g* for 10 min, and stored in PBS.

T Cell Characterization

T cells were stained with APC anti-mouse CD3ε clone 145-2C11 (0.2 mg/ml, #100311), APC/Cy7 anti-mouse CD4 clone GK1.5 (0.2 mg/mL, #100413), PerCP/Cy5.5 anti-mouse CD8a clone

53-6.7 (0.2 mg/ml, #100733), and PE anti-mouse CD25 clone 61 (0.2 mg/ml, #102007). All antibodies were obtained from BioLegend. The solutions were vortexed at 1,000 rpm and incubated for 30 min in the dark at RT. Next, PBS was added, vortexed, and spun down for 10 min (1,000 *g*) twice. Afterward, the pellet was resuspended in PBS and analyzed using the BD FACSCanto (BD Biosciences).

Statistical Analysis

Data are presented as mean ± SD and are either performed by technical or independent replicates (TR, IR) or by independent experiments (IE). ANOVA statistical tests were performed with Tukey post hoc tests if the samples were normally distributed and had equal variances. Otherwise, the Kruskal-Wallis statistical tests were performed with Dunn's test post hoc test. p values < 0.05 were considered statistically significant. Data were processed using GraphPad Prism version 5.00 for Windows (GraphPad Software).

SUPPLEMENTAL INFORMATION

Supplemental Information includes Supplemental Experimental Procedures and two figures and can be found with this article online at http://dx.doi.org/10.1016/j.stemcr.2015.10.018.

ACKNOWLEDGMENTS

The authors thank A. Van Santvoort and T. Buelens for their help in data acquisition and processing and H. Grosemans for her help in maintaining the animal colonies and molecular analyses. The radiopharmacy team from the Nuclear Medicine Department at UZ Leuven is acknowledged for $^{99m}TcO_4^-$ tracer preparations. B.H. is the recipient of a research grant from the IWT-Vlaanderen. O.G. is a senior clinical investigator of the Fund for Scientific Research Flanders (1831812N). The M.S. Laboratory is supported by the Opening the Future Campaign EJJ-OPTFUT-02010 and FWO (#G060612N, #G0A8813N, and #G088715N). M.S. and C.M.V. would also like to thank Rondoufonds voor Duchenne Onderzoek for the kind donation. The C.M.V. Laboratory is supported by SBO-BRAINSTEM (#60838). We also acknowledge infrastructural funding by the InfraMouse Grant from the Hercules Foundation (ZW09-03).

Received: July 22, 2015
Revised: October 29, 2015
Accepted: October 29, 2015
Published: November 25, 2015

REFERENCES

Adriouch, S., Franck, E., Drouot, L., Bonneau, C., Jolinon, N., Salvetti, A., and Boyer, O. (2011). Improved immunological tolerance following combination therapy with CTLA-4/Ig and AAV-mediated PD-L1/2 muscle gene transfer. Front Microbiol. *2*, 199.

Alpdogan, O. (2013). Advances in immune regulation in transplantation. Discov. Med. *15*, 150–159.

Anderton, S.M., and Liblau, R.S. (2008). Regulatory T cells in the control of inflammatory demyelinating diseases of the central nervous system. Curr. Opin. Neurol. *21*, 248–254.

Boise, L.H., Minn, A.J., Noel, P.J., June, C.H., Accavitti, M.A., Lindsten, T., and Thompson, C.B. (1995). CD28 costimulation can promote T cell survival by enhancing the expression of Bcl-XL. Immunity *3*, 87–98.

Bushby, K., Finkel, R., Birnkrant, D.J., Case, L.E., Clemens, P.R., Cripe, L., Kaul, A., Kinnett, K., McDonald, C., Pandya, S., et al.; DMD Care Considerations Working Group (2010). Diagnosis and management of Duchenne muscular dystrophy, part 1: diagnosis, and pharmacological and psychosocial management. Lancet Neurol. *9*, 77–93.

Chung, J.K. (2002). Sodium iodide symporter: its role in nuclear medicine. J. Nucl. Med. *43*, 1188–1200.

Cossu, G., Previtali, S.C., Napolitano, S., Cicalese, M.P., Tedesco, F.S., Nicastro, F., Noviello, M., Roostalu, U., Natali Sora, M.G., Scarlato, M., et al. (2015). Intra-arterial transplantation of HLA-matched donor mesoangioblasts in Duchenne muscular dystrophy. EMBO Mol Med. Published online November 5, 2015. http://dx.doi.org/10.15252/emmm.201505636.

Duclos, F., Straub, V., Moore, S.A., Venzke, D.P., Hrstka, R.F., Crosbie, R.H., Durbeej, M., Lebakken, C.S., Ettinger, A.J., van der Meulen, J., et al. (1998). Progressive muscular dystrophy in alpha-sarcoglycan-deficient mice. J. Cell Biol. *142*, 1461–1471.

English, K., Tonlorenzi, R., Cossu, G., and Wood, K.J. (2013). Mesoangioblasts suppress T cell proliferation through IDO and PGE-2-dependent pathways. Stem Cells Dev. *22*, 512–523.

Everaert, B.R., Bergwerf, I., De Vocht, N., Ponsaerts, P., Van Der Linden, A., Timmermans, J.P., and Vrints, C.J. (2012). Multimodal in vivo imaging reveals limited allograft survival, intrapulmonary cell trapping and minimal evidence for ischemia-directed BMSC homing. BMC Biotechnol. *12*, 93.

Fischer, L., Trunečka, P., Gridelli, B., Roy, A., Vitale, A., Valdivieso, A., Varo, E., Seehofer, D., Lynch, S., Samuel, D., et al. (2011). Pharmacokinetics for once-daily versus twice-daily tacrolimus formulations in de novo liver transplantation: a randomized, open-label trial. Liver Transpl. *17*, 167–177.

Gambhir, S.S., Barrio, J.R., Herschman, H.R., and Phelps, M.E. (1999). Assays for noninvasive imaging of reporter gene expression. Nucl. Med. Biol. *26*, 481–490.

George, J.F., Gooden, C.W., Guo, L., and Kirklin, J.K. (2008). Role for CD4(+)CD25(+) T cells in inhibition of graft rejection by extracorporeal photopheresis. J. Heart Lung Transplant. *27*, 616–622.

Gheysens, O., Lin, S., Cao, F., Wang, D., Chen, I.Y., Rodriguez-Porcel, M., Min, J.J., Gambhir, S.S., and Wu, J.C. (2006). Noninvasive evaluation of immunosuppressive drug efficacy on acute donor cell survival. Mol. Imaging Biol. *8*, 163–170.

Guttinger, M., Tafi, E., Battaglia, M., Coletta, M., and Cossu, G. (2006). Allogeneic mesoangioblasts give rise to alpha-sarcoglycan expressing fibers when transplanted into dystrophic mice. Exp. Cell Res. *312*, 3872–3879.

Huber, B.C., Ransohoff, J.D., Ransohoff, K.J., Riegler, J., Ebert, A., Kodo, K., Gong, Y., Sanchez-Freire, V., Dey, D., Kooreman, N.G., et al. (2013). Costimulation-adhesion blockade is superior to cyclosporine A and prednisone immunosuppressive therapy for preventing rejection of differentiated human embryonic stem cells following transplantation. Stem Cells *31*, 2354–2363.

Kitchens, W.H., Haridas, D., Wagener, M.E., Song, M., Kirk, A.D., Larsen, C.P., and Ford, M.L. (2012). Integrin antagonists prevent costimulatory blockade-resistant transplant rejection by CD8(+) memory T cells. Am. J. Transplant. *12*, 69–80.

Krönke, M., Leonard, W.J., Depper, J.M., Arya, S.K., Wong-Staal, F., Gallo, R.C., Waldmann, T.A., and Greene, W.C. (1984). Cyclosporin A inhibits T-cell growth factor gene expression at the level of mRNA transcription. Proc. Natl. Acad. Sci. USA *81*, 5214–5218.

Lee, H.W., Jeon, Y.H., Hwang, M.H., Kim, J.E., Park, T.I., Ha, J.H., Lee, S.W., Ahn, B.C., and Lee, J. (2013). Dual reporter gene imaging for tracking macrophage migration using the human sodium iodide symporter and an enhanced firefly luciferase in a murine inflammation model. Mol. Imaging Biol. *15*, 703–712.

Lee, A.R., Woo, S.K., Kang, S.K., Lee, S.Y., Lee, M.Y., Park, N.W., Song, S.H., Lee, S.Y., Nahm, S.S., Yu, J.E., et al. (2015a). Adenovirus-mediated expression of human sodium-iodide symporter gene permits in vivo tracking of adipose tissue-derived stem cells in a canine myocardial infarction model. Nucl. Med. Biol. *42*, 621–629.

Lee, H.W., Yoon, S.Y., Singh, T.D., Choi, Y.J., Lee, H.J., Park, J.Y., Jeong, S.Y., Lee, S.W., Ha, J.H., Ahn, B.C., et al. (2015b). Tracking of dendritic cell migration into lymph nodes using molecular imaging with sodium iodide symporter and enhanced firefly luciferase genes. Sci. Rep. *5*, 9865.

Li, Z., Suzuki, Y., Huang, M., Cao, F., Xie, X., Connolly, A.J., Yang, P.C., and Wu, J.C. (2008). Comparison of reporter gene and iron particle labeling for tracking fate of human embryonic stem cells and differentiated endothelial cells in living subjects. Stem Cells *26*, 864–873.

Massoud, T.F., and Gambhir, S.S. (2003). Molecular imaging in living subjects: seeing fundamental biological processes in a new light. Genes Dev. *17*, 545–580.

Minn, I., Menezes, M.E., Sarkar, S., Yarlagadda, K., Das, S.K., Emdad, L., Sarkar, D., Fisher, P.B., and Pomper, M.G. (2014). Molecular-genetic imaging of cancer. Adv. Cancer Res. *124*, 131–169.

Murakami, N., and Riella, L.V. (2014). Co-inhibitory pathways and their importance in immune regulation. Transplantation *98*, 3–14.

Nicolls, M.R., Coulombe, M., Yang, H., Bolwerk, A., and Gill, R.G. (2000). Anti-LFA-1 therapy induces long-term islet allograft acceptance in the absence of IFN-gamma or IL-4. J. Immunol. *164*, 3627–3634.

Noviello, M., Tedesco, F.S., Bondanza, A., Tonlorenzi, R., Rosaria Carbone, M., Gerli, M.F., Marktel, S., Napolitano, S., Cicalese, M.P., Ciceri, F., et al. (2014). Inflammation converts human mesoangioblasts into targets of alloreactive immune responses: implications for allogeneic cell therapy of DMD. Mol. Ther. *22*, 1342–1352.

Odintsov, B., Chun, J.L., Mulligan, J.A., and Berry, S.E. (2011). 14.1 T whole body MRI for detection of mesoangioblast stem cells in a murine model of Duchenne muscular dystrophy. Magn. Reson. Med. *66*, 1704–1714.

Patel, J.K., and Kobashigawa, J.A. (2004). Cardiac transplant experience with cyclosporine. Transplant. Proc. *36* (2, Suppl), 323S–330S.

Quattrocelli, M., Costamagna, D., Giacomazzi, G., Camps, J., and Sampaolesi, M. (2014). Notch signaling regulates myogenic regenerative capacity of murine and human mesoangioblasts. Cell Death Dis. *5*, e1448.

Rosenberg, A.S., Mizuochi, T., Sharrow, S.O., and Singer, A. (1987). Phenotype, specificity, and function of T cell subsets and T cell interactions involved in skin allograft rejection. J. Exp. Med. *165*, 1296–1315.

Sakaguchi, S., Sakaguchi, N., Asano, M., Itoh, M., and Toda, M. (1995). Immunologic self-tolerance maintained by activated T cells expressing IL-2 receptor alpha-chains (CD25). Breakdown of a single mechanism of self-tolerance causes various autoimmune diseases. J. Immunol. *155*, 1151–1164.

Sakuma, T., Barry, M.A., and Ikeda, Y. (2012). Lentiviral vectors: basic to translational. Biochem. J. *443*, 603–618.

Sampaolesi, M., Torrente, Y., Innocenzi, A., Tonlorenzi, R., D'Antona, G., Pellegrino, M.A., Barresi, R., Bresolin, N., De Angelis, M.G., Campbell, K.P., et al. (2003). Cell therapy of alpha-sarcoglycan null dystrophic mice through intra-arterial delivery of mesoangioblasts. Science *301*, 487–492.

Sampaolesi, M., Blot, S., D'Antona, G., Granger, N., Tonlorenzi, R., Innocenzi, A., Mognol, P., Thibaud, J.L., Galvez, B.G., Barthélémy, I., et al. (2006). Mesoangioblast stem cells ameliorate muscle function in dystrophic dogs. Nature *444*, 574–579.

Schiff, M., Keiserman, M., Codding, C., Songcharoen, S., Berman, A., Nayiager, S., Saldate, C., Aranda, R., Becker, J.C., Nys, M., et al. (2011). Clinical response and tolerability to abatacept in patients with rheumatoid arthritis previously treated with infliximab or abatacept: open-label extension of the ATTEST Study. Ann. Rheum. Dis. *70*, 2003–2007.

Strom, T.B., Tilney, N.L., Carpenter, C.B., and Busch, G.J. (1975). Identity and cytotoxic capacity of cells infiltrating renal allografts. N. Engl. J. Med. *292*, 1257–1263.

Templin, C., Zweigerdt, R., Schwanke, K., Olmer, R., Ghadri, J.R., Emmert, M.Y., Müller, E., Küest, S.M., Cohrs, S., Schibli, R., et al. (2012). Transplantation and tracking of human-induced pluripotent stem cells in a pig model of myocardial infarction: assessment of cell survival, engraftment, and distribution by hybrid single photon emission computed tomography/computed tomography of sodium iodide symporter transgene expression. Circulation *126*, 430–439.

Vincenti, F., Mendez, R., Pescovitz, M., Rajagopalan, P.R., Wilkinson, A.H., Butt, K., Laskow, D., Slakey, D.P., Lorber, M.I., Garg, J.P., and Garovoy, M. (2007). A phase I/II randomized open-label multicenter trial of efalizumab, a humanized anti-CD11a, anti-LFA-1 in renal transplantation. Am. J. Transplant. *7*, 1770–1777.

Wolfs, E., Holvoet, B., Gijsbers, R., Casteels, C., Roberts, S.J., Struys, T., Maris, M., Ibrahimi, A., Debyser, Z., Van Laere, K., et al. (2014). Optimization of multimodal imaging of mesenchymal stem cells using the human sodium iodide symporter for PET and Cerenkov luminescence imaging. PLoS ONE *9*, e94833.